Electrical Power and Energy Systems 47 (2013) 264–279

Contents lists available at SciVerse ScienceDirect

Electrical Power and Energy Systems

journal homepage: www.elsevier.com/locate/ijepes

Direct synchronous-asynchronous conversion system for hybrid electrical vehicle applications. An energy-based modeling approach

Raúl S. Muñoz-Aguilar [a,*], Arnau Dòria-Cerezo [b], Paul F. Puleston [c,d]

[a] Universitat Politècnica de Catalunya, Department of Electrical Engineering, 08222 Terrassa, Spain
[b] Universitat Politècnica de Catalunya, Department of Electrical Engineering and Institute of Control Engineering, 08800 Vilanova i la Geltrú, Spain
[c] CONICET and LEICI, National University of La Plata, CC91, 1900, La Plata, Argentina
[d] Marie Curie Fellow, IRI, CSIC-UPC, Barcelona, Spain

ARTICLE INFO

Article history:
Received 9 June 2012
Received in revised form 5 November 2012
Accepted 9 November 2012
Available online 12 December 2012

Keywords:
AC machines
Hybrid electric vehicle
Modeling

ABSTRACT

This paper presents a proposal for a series hybrid electric vehicle propulsion system. This new configuration is based on a wound-rotor synchronous generator (WRSM) and a doubly-fed induction machine (DFIM). The energy-based model of the whole system is obtained taking advantage of the capabilities of the port-based modeling techniques. From the *dq* port-controlled Hamiltonian description of the WRSM and DFIM, the Hamiltonian model of the proposed Direct Synchronous-Asynchronous Conversion System (DiSAC) is developed. Subsequently, the bond graph models of the DiSAC and associate systems are also provided. Numerical simulations are also presented in order to validate the proposed system.

1. Introduction

Hybrid electrical vehicles (HEV) are the focus of many research interests because they are able to provide good performance and long operating time [1,2]. Basically, the HEV is composed of an internal combustion engine, an electrical machine and a battery pack or ultracapacitor storage system [3]. The main goal of this structure is to reduce the CO_2 emissions by means of the regenerative breaking using the electrical machine, both as a motor drive or as a generator, which charges or discharges the batteries. It is also desired to keep the drivability performance of the vehicle [4]. Depending on the topology, HEV can be divided into two basic configurations: parallel and series.

In this work we focus on the advanced topologies of series HEV. Wound-rotor electrical machines have the ability to control them trough the rotor windings. It offers several advantages as the size of the power converter could be smaller than a direct connection to the stator side.

The use of wound-rotor machines (as doubly-fed induction machines) has been studied as a part of a power train [5,6]. However, examples in [5,6] had some performance limitations because they are unable to control intermediate variables between both machines (power factor, reactive power or stator voltage). More control inputs are necessary in order to achieve a good control for the HEV purposes (for instance, the stator reactive power between both machines cannot be controlled with the previous schemes). The propulsion system we propose consists of a wound-rotor synchronous generator (WRSM) and a doubly-fed induction machine (DFIM), and it is an improved version of the topology proposed in [7]. The main advantage of this configuration is the ability to manage the energy without a full power converter between both machines. In this case the power management is done through the stator and rotor voltages of the DFIM and the field voltage of the WRSM. This configuration of two machines with wounded rotor allows to use smaller power converters than the conventional topology [4], also increasing the number of control actions and, consequently, a better power management can be done.

Several modeling and simulation tools have been employed in this field [8,9]. In particular, a powerful modeling approach potentially suitable to deal with the inherent features of the proposed HEV system is the one provided by network modeling. Network modeling is a prevailing trend in the description of physical systems for analysis, control applications and simulation. The system is split into open subsystems (tearing), the subsystems are modeled (zooming), and the model of the overall system is obtained by interconnecting the models of the subsystems (linking) [10]. The main advantage of such approach is that the models of the physical subsystems can be stored in libraries. The modeling process can be performed in an iterative manner and the model of the overall system is simply constructed by interconnecting the library sub-models.

* Corresponding author. Tel.: +34 690804574.
E-mail addresses: raul.munoz-aguilar@upc.edu (R.S. Muñoz-Aguilar), arnau.doria@upc.edu (A. Dòria-Cerezo), puleston@ing.unlp.edu.ar (P.F. Puleston).

0142-0615/$ - see front matter © 2012 Elsevier Ltd. All rights reserved.
http://dx.doi.org/10.1016/j.ijepes.2012.11.012

Specifically, Energy-based modeling (EBM) is a network modeling technique which describes dynamical systems from a physical point of view, representing the power flowing between the different elements and where the energy is stored and dissipated. A recent implementation of this idea is known as port Hamiltonian systems or port-controlled Hamiltonian systems (PCHS), see [11,12]. One of the strong aspects of the PCHS is that a power-preserving interconnection between port-Hamiltonian systems results in another port-Hamiltonian system with composite energy, dissipation, and interconnection structure. Based on this principle, complex, multidomain systems can be modeled by interconnecting port-Hamiltonian descriptions of its subsystems.

PCHS theory provides the mathematical foundation of the bond graph approach, which allows to model dynamical systems graphically, describing the energy flowing through different elements, which represents source, storage, dissipative and transmission elements [13]. The bond graph description easily permits the integration of submodels and, by means of a simple computer algorithm, the simulation-ready equations of a complex model can be derived.

In this paper, a new configuration for a HEV propulsion system is presented and the dynamical model of the power train is obtained in the port-controlled Hamiltonian and bond graph descriptions. Finally, some simulations are performed to evaluate the propulsion system under a standard driving test profile.

2. System description

2.1. State of the art

Fig. 1a shows the classic configuration of a series HEV [4,14]. It contains an internal combustion engine (E), two electrical machines (G and M) connected by a power converter (P) which also is connected to the batteries (B). Series HEV offers several advantages; the internal combustion engine (ICE) is mechanically decoupled from the transmission, the final torque is given by an electrical machine and also simple management strategies can be adopted [15,16]. One of the disadvantages of this topology is that all the power flows through the power converter and, consequently, the losses could be important.

Wound-rotor electrical machines offer the main advantage that the rotor voltages can be used for control purposes. Based on this, some previous works proposed DFIM as electrical machines for HEV applications [5,6], see Fig. 1b and c. The advantage of this kind of topologies is that a fractional power converter can be used instead of a full power one. Effectively, the stator power converter is replaced by a rotor power converter and, consequently, losses can be reduced. The so-called Joint System [5] used a DFIM as generator, with an induction machine as a motor. In [6], the Variable Voltage Variable Frequency scheme was introduced, with the DFIM as a motor with a permanent magnet synchronous machine (PMSM) for the generating part.

2.2. The DiSAC propulsion system

However, the topologies presented in Refs. [5,6] are not able to control efficiently the system reactive power and stator voltage amplitudes simultaneously. To overcome this drawback, a new topology for a series HEV called Direct Synchronous-Asynchronous Conversion System (DiSAC) is introduced in this paper.

Fig. 2 shows the electrical connection of the DiSAC system. The WRSM is mechanically connected with the ICE, and operates as a generator. The WRSM and DFIM stators are directly connected one to the other and the shaft of the DFIM is coupled to the HEV transmission. Notice that the DFIM can operate either in generator or motor mode. Both machines (WRSM and DFIM) are rotor connected to the batteries by means of DC/DC and AC/DC converters, respectively, and batteries are also connected to the stator side by means of a power converter.

This new scheme defines six control inputs: the field (or rotor) voltage of the WRSM, v_F, the two rotor dq-voltage components of the DFIM, $v_r \in \mathbb{R}^2$, the two dq-voltages generated by the power converter, $v_I \in \mathbb{R}^2$ and the mechanical torque produced by the ICE, τ_W. These six control variables are able to control the electrical torque produced by the DFIM, to manage the power flow, to keep a stator voltage to its nominal value (together with a stator power factor close to one) and allows to extract or inject power to the machines stator.

In order to simplify the problem, the controllers can be designed independently for each machine and the stator power converter. With this premise, the stator voltage amplitude can be controlled by the field rotor of the WRSM. Using the DFIM rotor voltage, the output torque can be regulated, and an unitary power factor in the stator side can be obtained. The ICE torque can regulate the WRSM speed to work in an optimal operation zone and, finally, the stator power converter can be in charge of inject or extract active power into the machines stator, and to regulate the power management of the system.

With respect to the classical series topology, the presented configuration has the advantage that the power converters required to control both machines are considerably smaller than the classic back-to-back converter. Furthermore, this topology offers enough control inputs for an appropriate power management which includes the regenerative breaking.

2.3. Power flow operation

The power flow operation is illustrated in Fig. 3. Thanks to the use of wounded electrical machines, the power is mainly flowing through the WRSM, the DFIM and the power inverter, and the energy required by the fractional DC/DC and AC/DC converters is relatively small, see simulation results in Section 6.

The WRSM only acts as a generator with a mechanical incoming power, P_{mW}, and provides an electrical power, P_{sW}. Both are related by

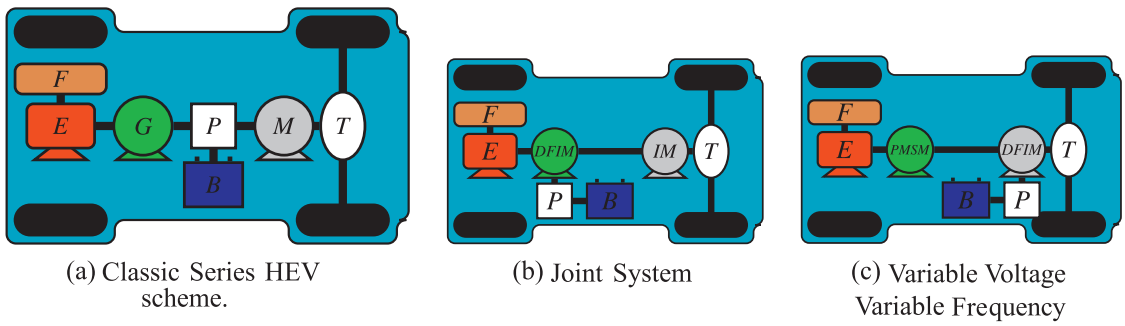

Fig. 1. Classic and advanced series HEV schemes.

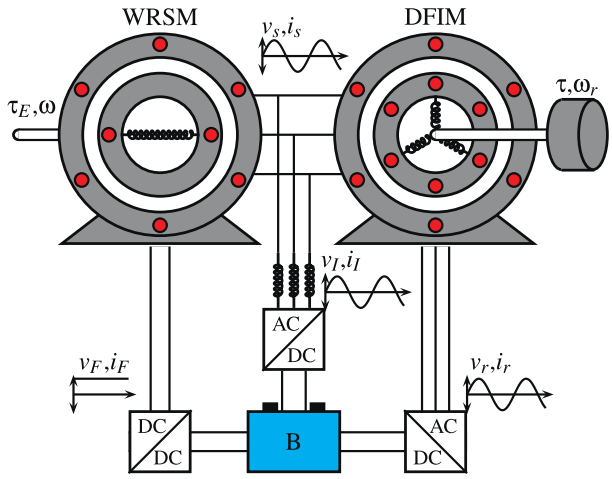

Fig. 2. Electrical scheme of the DiSAC system.

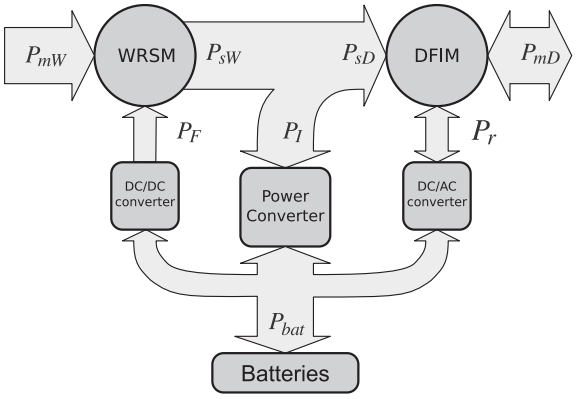

Fig. 3. Power flow diagram of the DiSAC propulsion system.

$$P_{mW} = P_{sW} - R_{sW}|i_{sW}|^2 - B_W\omega_W^2 \tag{1}$$

where the terms $R_{sW}|i_{sW}|^2$ and $B_W\omega_W^2$ represents the ohmic and mechanical losses. The field power required is

$$P_F = R_F i_F^2. \tag{2}$$

Similarly to the WRSM, the DFIM stator power flows are given by

$$P_{sD} = P_{mD} - R_{sD}|i_{sD}|^2 - B_D\omega_D^2 \tag{3}$$

where P_{sD} is the power flowing through the stator side, P_{mD} is the delivered mechanical power, and $R_{sD}|i_{sD}|^2$, $B_D\omega_D^2$ represents the ohmic and mechanical losses. The DFIM rotor power is

$$P_r = (\omega_s - \omega_D)\tau_D - R_r|i_r|^2, \tag{4}$$

where the $R_r|i_r|^2$ term are the ohmic losses. Notice that P_r strongly depend on the slip. So, to reduce it, it would be desirable to regulate the WRSM speed, ω_s close to ω_D keeping the ICE within the range allowing to have the higher efficiency. See further details of the power analysis in [17].

In a regenerative breaking mode, the kinetic energy recovered flows from the DFIM to the batteries through the power converter.

3. Port controlled Hamiltonian model

In this section, the port-controlled Hamiltonian model of the proposed series HEV DiSAC configuration is derived interconnecting the standard *dq* models of the DFIM, WRSM and the inverter with a battery model by means of power converters.

Hamiltonian modeling uses state dependent energy functions to characterize the dynamics of the different subsystems, and connects them using a Dirac structure, which embodies the power preserving network of relationships established by the corresponding physical laws. The result is a mathematical model with a specific structure, called port-controlled Hamiltonian system (PCHS) [11], which lends itself to a natural, physics-based analysis and control design.

An explicit PCHS has the form

$$\begin{cases} \dot{x} = (\mathcal{J}(x) - \mathcal{R}(x))\partial H + \mathcal{G}(x)u \\ y = \mathcal{G}^T(x)\partial H \end{cases} \tag{5}$$

where $x \in \mathbb{R}^n$ are the energy variables (or state vector), $u, y \in \mathbb{R}^m$ are the port variables, and $H(x) : \mathbb{R}^n \to \mathbb{R}$ is the Hamiltonian function, representing the energy function of the system. The ∂_x (or ∂, if no confusion arises) operator defines the gradient of a function of x and, in the sequel, we will take it as a column vector. $\mathcal{J}(x) \in \mathbb{R}^{n\times n}$ is the interconnection matrix, which is skew-symmetric ($\mathcal{J}(x) = -\mathcal{J}(x)^T$), representing the internal energy flow in the system, and $\mathcal{R}(x) \in \mathbb{R}^{n\times n}$ is the dissipation matrix, symmetric and, in physical systems, positive semidefinite ($\mathcal{R}(x) = \mathcal{R}(x)^T \geqslant 0$), which accounts for the internal losses of the system. Finally, $\mathcal{G}(x) \in \mathbb{R}^{n\times m}$ is an interconnection matrix describing the port connection of the system to the outside world. It yields the flow of energy to/from the system through the port variables, u and y, which are conjugated, i.e. their dot product has units of power.

Usually, three-phase electrical machine modeling uses the so-called Park (or *dq*) transformation. This mathematical transformation allows to decouple variables and to facilitate the solution of difficult equations which depends on the rotor position [18]. With the *dq* transformation the *abc* three-phase variables (voltages and currents) are reduced to a two-phase *dq* variables (assuming that the homopolar component is equal to zero due to the existence of a balanced system). The reference frame for the Park transformation depends on the application.

In this case, the selected reference is the mechanical angle of the WRSM. In the sequel, machines of one pair of poles are considered. Note that in such case the mechanical speed of the synchronous machine, ω_W, matches the stator frequency, ω_s.

3.1. PCHS of a doubly-fed induction machine

The PCHS of a doubly-fed induction machine has been presented in [19]. The dynamics is given by

$$\dot{x}_D = (\mathcal{J}_D(x) - \mathcal{R}_D)\partial H_D + \mathcal{G}_D u_D. \tag{6}$$

The Hamiltonian variables are

$$x_D^T = [\lambda_{sD}^T, \lambda_r^T, p_D],$$

where $\lambda_{sD} = [\lambda_{sDd}, \lambda_{sDq}]^T$ and $\lambda_r = [\lambda_{rd}, \lambda_{rq}]^T$ are the stator and rotor fluxes in *dq*-coordinates, respectively, $p_D = J_D\omega_D$ is the mechanical momentum, ω_D is the mechanical speed and J_D is the inertia of the rotating parts. The *D* subindex has been included to refer to the DFIM.

The interconnection and damping matrices are, respectively,

$$\mathcal{J}_D(x) = \begin{bmatrix} -\omega_s L_{sD} J_2 & -\omega_s L_{sr} J_2 & 0 \\ -\omega_s L_{sr} J_2 & -(\omega_s - \omega_D) L_r J_2 & L_{sr} J_2 i_{sD} \\ 0 & L_{sr} i_{sD}^T J_2 & 0 \end{bmatrix}$$

$$\mathcal{R}_D = \begin{bmatrix} R_{sD} I_2 & 0 & 0 \\ 0 & R_r I_2 & 0 \\ 0 & 0 & B_D \end{bmatrix}$$

where $i_{sD}, i_r \in \mathbb{R}^2$ are the stator and rotor currents, R and L are resistance and inductances,[1] ω_s is the stator electric frequency, B_D is the mechanical damping, and

$$J_2 = \begin{bmatrix} 0 & -1 \\ 1 & 0 \end{bmatrix}, \quad I_2 = \begin{bmatrix} 1 & 0 \\ 0 & 1 \end{bmatrix}.$$

To simplify the notation, 0 represents a zero matrix with the appropriate dimension.

Considering that all the elements are linear, Hamiltonian variables (fluxes and momentum) are related with currents and mechanical speed by

$$x_D = \mathcal{L}_D \begin{bmatrix} i_{sD} \\ i_r \\ \omega_D \end{bmatrix} \tag{7}$$

where

$$\mathcal{L}_D = \begin{bmatrix} L_{sD} I_2 & L_{sr} I_2 & 0 \\ L_{sr} I_2 & L_r I_2 & 0 \\ 0 & 0 & J_D \end{bmatrix}.$$

The port connection, $\mathcal{G}_D$, is 5×5 identity matrix, with the port variables $u_D^T = [v_{sD}^T, v_r^T, \tau_D]$, where $v_{sD}, v_r \in \mathbb{R}^2$ are the stator and rotor voltages and τ_D is an external torque. The Hamiltonian model is completed with the energy function

$$H_D(x_D) = \frac{1}{2} x_D^T \mathcal{L}_D^{-1} x_D.$$

Notice that the variables obtained operating ∂H_D is a vector with the stator and rotor currents and the mechanical speed.

3.2. PCHS of a wound-rotor synchronous machine

A Port-controlled Hamiltonian model of a synchronous machine with permanent magnets, can be found in [20]. However, the wound rotor synchronous machine includes a rotor winding which has to be considered. Then, the PCHS is

$$\dot{x}_W = (\mathcal{J}_W(x) - \mathcal{R}_W)\partial H_W + \mathcal{G}_W u_W, \tag{8}$$

with

$$x_W^T = [\lambda_{sW}^T, \lambda_F, p_W],$$

where $\lambda_{sW} = [\lambda_{sWd}, \lambda_{sWq}]^T$ is the stator inductor flux in dq-coordinates, λ_F is the rotor (or field) inductor flux, $p_W = J_W \omega_W$ is the mechanical momentum, ω_W is the mechanical speed, and J_W is the inertia of the rotating parts. In this case, the W subindex has been included to refer to the WRSM.

The interconnection and damping matrices are, respectively,

$$\mathcal{J}_W = \begin{bmatrix} -\omega_W L_{sW} J_2 & 0 & -M i_F \\ 0 & 0 & 0 \\ M^T i_F & 0 & 0 \end{bmatrix}$$

$$\mathcal{R}_W = \begin{bmatrix} R_{sW} I_2 & 0 & 0 \\ 0 & R_F & 0 \\ 0 & 0 & B_W \end{bmatrix}$$

where $i_{sW} \in \mathbb{R}^2$ are the stator currents, i_F is the rotor (or field) current, R and L are resistance and inductances,[2] B_W is the mechanical damping and

$$M = \begin{bmatrix} 0 \\ L_m \end{bmatrix}$$

with L_m being the mutual inductance.

Similarly to the DFIM, for a linear case the WRSM fluxes and momentum are related with currents and mechanical speed by

$$\lambda_W = \mathcal{L}_W \begin{bmatrix} i_{sW} \\ i_F \\ \omega_W \end{bmatrix} \tag{9}$$

and the inductance matrix, $\mathcal{L}_W$, is

$$\mathcal{L}_W = \begin{bmatrix} L_{sW} I_2 & M & 0 \\ M^T & L_F & 0 \\ 0 & 0 & J_W \end{bmatrix}.$$

The port connection, $\mathcal{G}_W$, is represented by an identity 4×4 matrix, with the port variables $u_W^T = [v_{sW}^T, v_F, \tau_W]$, where $v_{sW} \in \mathbb{R}^2$ is the stator voltages, v_F is the rotor (or field) voltage, and τ_W is the applied external torque. Finally, the Hamiltonian function is

$$H_W(x_W) = \frac{1}{2} x_W^T \mathcal{L}_W^{-1} x_W.$$

3.3. PCHS of a three-phase DC/AC inverter

As a first approximation, and neglecting the effect of switches, the three-phase DC/AC inverter can be modeled as a couple of voltage sources in series with an RL element. Then, the PCHS takes the form

$$\dot{x}_I = (\mathcal{J}_I - \mathcal{R}_I)\partial H_I + \mathcal{G}_I u_I, \tag{10}$$

where the state are the inductor fluxes $x_I^T = [\lambda_{Id}, \lambda_{Iq}] \in \mathbb{R}^2$. The interconnection matrix reflects the effect of the rotation in the Park coordinates

$$\mathcal{J}_I = -\omega_I L_I J_2,$$

where ω_I is the frequency of the generated AC voltage, L_I is the inductance parameter, and the losses corresponds to the parasitic resistive effects contained in the dissipation matrix

$$\mathcal{R}_I = R_I I_2.$$

The port variables, $u_I^T = [e_I^T, v_I^T]$, comprise the generated voltages by the switching policy, $e_I^T = [e_{Id}, e_{Iq}] \in \mathbb{R}^2$, and the inverter voltages, $v_I^T = [v_{Id}, v_{Iq}] \in \mathbb{R}^2$, which are connected to the dynamics with

$$\mathcal{G}_I = [I_2 \quad I_2]. \tag{11}$$

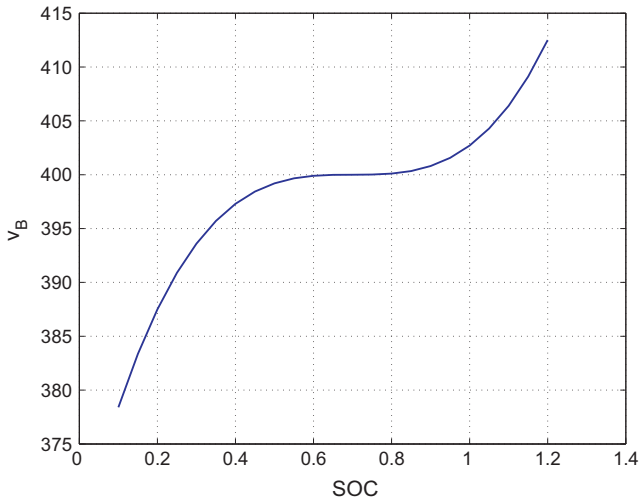

Fig. 4. The SOC versus battery voltage.

[1] Subscripts s and r refer to stator and rotor respectively.

[2] Subscripts s and F refer to stator and field respectively.

Fluxes are defined as

$$x_I = L_I i_I,$$

where $i_I^T = [i_{Id}, i_{Iq}] \in \mathbb{R}^2$ are the inductor currents. The Hamiltonian function is

$$H_I(x_I) = \frac{1}{2} x_I^T \mathcal{L}_I^{-1} x_I.$$

3.4. PCHS of a battery

A battery (lead–acid or lithium–ion, among others) is an energy storage device which involves electrochemical reactions and complex dynamics [4]. In this paper, a simplified model of a battery is adopted which, thanks to the network modeling basis of the PCHS, can be easily replaced by a complex model if necessary.

The battery model consists of a nonlinear capacitor in parallel with a resistance, yielding a first order nonlinear system, which can be represented in a PCHS form with

$$\dot{x}_B = -R_B \partial H_B + G_B u_B \tag{12}$$

where $x_B = q_B$ is the state of charge (SOC), R_B models the self-discharge, $G_B = b_1$ scales the charge to p.u. (or percent units, depending on the used model), and the input corresponds to the incoming current, $u_B = i_B$. Note that, as the battery is a one-dimensional system, the interconnection matrix is null, $J_B = 0$. The Hamiltonian function,

$$H_B = \frac{1}{4} b_2 (x_B - b_3)^4 + b_4 x_B \tag{13}$$

where $x_B > 0$, contains the nonlinear relationship between the SOC and the battery voltage, v_B, by means of the output equation

$$y_B = G_B \partial H_B \tag{14}$$

where $y_B = v_B$. From the latter, the SOC and the voltage battery are related by

$$v_B = b_2 (x_B - b_3)^3 + b_4. \tag{15}$$

Fig. 4 shows the battery voltage versus the SOC (15), with the following parameters $b_2 = 100$, $b_3 = 0.7$ and $b_4 = 400$. Realistic approximations to an industrial battery can be obtained modifying the Hamiltonian function (13), or interconnecting several cell models.

3.5. The overall system

The whole system is obtained linking the aforementioned subsystems. Fig. 2 shows how they are interconnected. The machines are connected through the stator windings together with the power converter. Then, the link of the DC/AC power converter and the electrical machines subsystems is achieved by setting the Kirchhoff voltage law

$$v_{sD} = v_{sW} = v_I, \tag{16}$$

and the Kirchhoff current law,

$$i_{sD} + i_{sW} + i_I = 0. \tag{17}$$

Also, the interconnection implies a common frequency,

$$\omega_s = \omega_W = \omega_I. \tag{18}$$

Also, the rotor windings of both WRSG and DFIM, and the inverter, are connected to the battery by means of power converters that manage the power flowing through the system. Power converters are modeled as ideal switches that relate the voltages and currents as follows

$$v_F = \mu_W v_B \tag{19}$$

$$i_{BW} = \mu_W i_F \tag{20}$$

$$v_r = \mu_D v_B \tag{21}$$

$$i_{BD} = \mu_D^T i_r \tag{22}$$

$$e_I = \mu_I v_B \tag{23}$$

$$i_{BI} = \mu_I^T i_I \tag{24}$$

where μ_W is the switch position of the DC–DC power converter, $\mu_D, \mu_I \in \mathbb{R}^2$ are the switching policy of the DC–AC inverters in the dq-coordinates (see examples in [21]), and i_{BW}, i_{BD}, i_{BI} are the currents in the battery side of the power converters that are related with the battery current by

$$i_B = -(i_{BD} + i_{BW} + i_{BI}). \tag{25}$$

Using (20), (22) and (24) in (25) and the Hamiltonan functions H_W, H_D and H_I

$$i_B = -\Gamma_D^T \partial H_D - \Gamma_W^T \partial H_W - \mu_I^T \partial H_I, \tag{26}$$

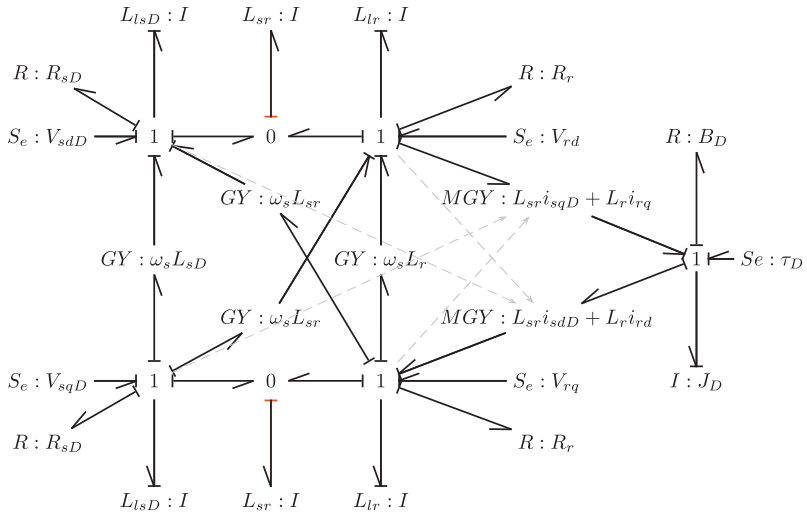

Fig. 5. Bond graph model of a doubly-fed induction machine.

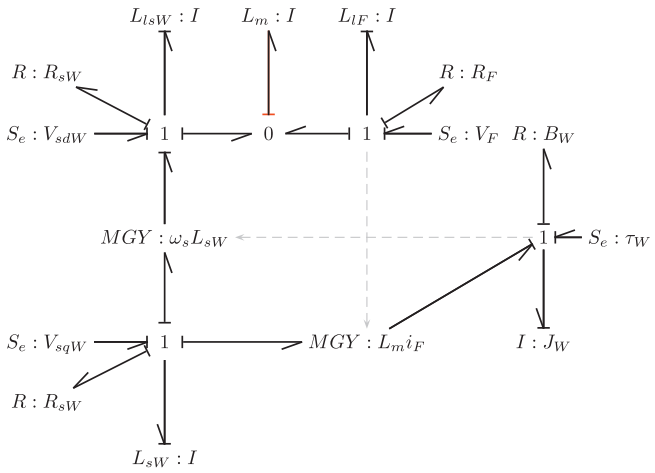

Fig. 6. Bond graph model of a wound-rotor synchronous machine.

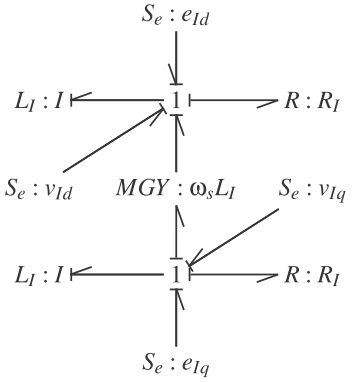

Fig. 7. Bond graph model of the stator inverter.

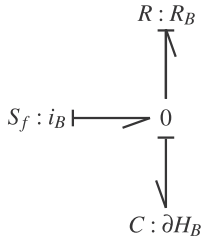

Fig. 8. Bond graph model of the battery.

where $\Gamma_D^T=[0,\mu_D^T,0]\in\mathbb{R}^5$ and $\Gamma_W^T=[0,\mu_W,0]\in\mathbb{R}^4$. Similarly with (19), (21), (23) and H_B

$$v_F=\mu_W\partial H_B \tag{27}$$
$$v_r=\mu_D\partial H_B \tag{28}$$
$$e_I=\mu_I\partial H_B. \tag{29}$$

This leads to the PCHS

$$\begin{bmatrix}\dot{x}_D\\ \dot{x}_W\\ \dot{x}_I\\ \dot{x}_B\end{bmatrix}=\begin{bmatrix}\mathcal{J}_D(x_D)-\mathcal{R}_D & 0 & 0 & \Gamma_D\\ 0 & \mathcal{J}_W(x_W)-\mathcal{R}_W & 0 & \Gamma_W\\ 0 & 0 & \mathcal{J}_I-\mathcal{R}_I & \mu_I\\ -\Gamma_D^T & -\Gamma_W^T & -\mu_I^T & -R_B\end{bmatrix}\begin{bmatrix}\partial H_D\\ \partial H_W\\ \partial H_I\\ \partial H_B\end{bmatrix}+\mathcal{B}v_I+\mathcal{G}_c u \tag{30}$$

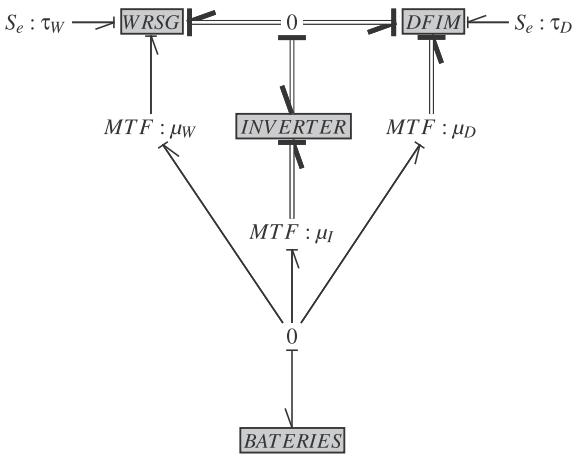

Fig. 9. Bond graph model of the complete system.

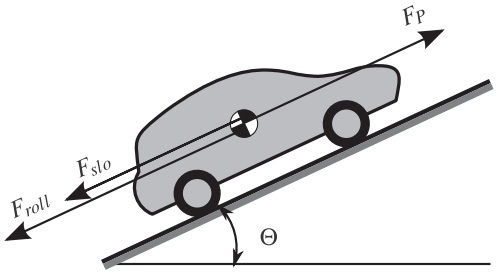

Fig. 10. Vehicle simplified model.

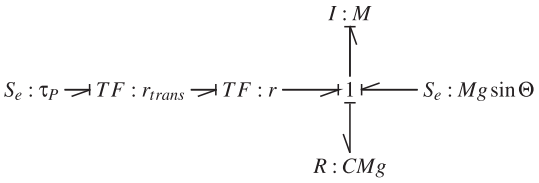

Fig. 11. Bond graph model of the vehicle dynamics.

with the external connection matrix,

$$\mathcal{G}_c^T=\begin{bmatrix}0&0&1&0&0&0&0&0\\0&0&0&0&0&1&0&0\end{bmatrix}\in\mathbb{R}^{2\times 12}, \tag{31}$$

the input port variables $u^T=[\tau_D,\tau_W]\in\mathbb{R}^2$, and the interconnection voltage constrain (16) is denoted in

$$\mathcal{B}^T=[I_2\quad 0\quad 0\quad I_2\quad 0\quad 0\quad I_2\quad 0]\in\mathbb{R}^{2\times 12}, \tag{32}$$

Note that the constraint on the currents (17), is represented by

$$0=\mathcal{B}^T\begin{bmatrix}\partial H_D\\ \partial H_W\\ \partial H_I\\ \partial H_B\end{bmatrix}. \tag{33}$$

The internal constraint voltage can be eliminated as follows. Let $\mathcal{B}^\perp$ denote a full-rank left annihilator[3] of $\mathcal{B}$,

[3] In general, a full-rank left annihilator of $\mathcal{B}\in\mathbb{R}^{n\times m}$, $\mathcal{B}^\perp$, implies: $\mathcal{B}^\perp\mathcal{B}=0$ and $\operatorname{rank}(\mathcal{B}^\perp)=n-m$.

$$\mathcal{B}^{\perp}=\begin{bmatrix} I_2 & 0 & 0 & 0 & 0 & 0 & -I_2 & 0\\ 0 & I_2 & 0 & 0 & 0 & 0 & 0 & 0\\ 0 & 0 & 1 & 0 & 0 & 0 & 0 & 0\\ 0 & 0 & 0 & I_2 & 0 & 0 & -I_2 & 0\\ 0 & 0 & 0 & 0 & 1 & 0 & 0 & 0\\ 0 & 0 & 0 & 0 & 0 & 1 & 0 & 0\\ 0 & 0 & 0 & 0 & 0 & 0 & 0 & 1 \end{bmatrix}. \tag{34}$$

Hence, premultiplying (30) with $\mathcal{B}^{\perp}$, and taking into account that the first and last dynamics are the same, the whole dynamics take the PCHS form

$$\dot{x}=(\mathcal{J}(x)-\mathcal{R})\partial H+\mathcal{G}u \tag{35}$$

with the new state defined by

$$x^T=\left[\lambda_{DI}^T,\lambda_r^T,p_D,\lambda_{IW}^T,\lambda_F,p_W,q_B\right],$$

where $\lambda_{DI}=\lambda_{sD}-\lambda_I$ and $\lambda_{WI}=\lambda_{sW}-\lambda_I$. The interconnection and dissipation matrices are (39) and (40), respectively, the energy function is the sum of H_D, H_W, H_I, and H_B, that can be written as

$$H(x)=\frac{1}{2}\lambda^T\mathcal{L}^{-1}\lambda+\frac{1}{2}J_D^{-1}p_D^2+\frac{1}{2}J_W^{-1}p_W^2+H_B(q_B), \tag{36}$$

where $\lambda^T=\left[\lambda_{DI}^T,\lambda_r^T,\lambda_{IW}^T,\lambda_F\right]$,

$$\mathcal{L}=\begin{bmatrix}(L_{sD}+L_I)I_2 & L_{sr}I_2 & L_II_2 & 0\\ L_{sr}I_2 & L_rI_2 & 0 & 0\\ L_II_2 & 0 & (L_{sW}+L_I)I_2 & M\\ 0 & 0 & M^T & L_F\end{bmatrix} \tag{37}$$

and the external connection matrix is

$$\mathcal{G}^T=\begin{bmatrix}0 & 0 & 1 & 0 & 0 & 0 & 0\\ 0 & 0 & 0 & 0 & 0 & 1 & 0\end{bmatrix}. \tag{38}$$

$$\mathcal{J}(x)=\begin{bmatrix}-\omega_s(L_{sD}+L_I)J_2 & -\omega_sL_{sr}J_2 & 0 & 0 & 0 & 0 & -\mu_I\\ -\omega_sL_{sr}J_2 & -(\omega_s-\omega_D)L_rJ_2 & L_{sr}J_2i_{sD} & 0 & 0 & 0 & \mu_D\\ 0 & L_{sr}i_{sD}^TJ_2 & 0 & 0 & 0 & 0 & 0\\ 0 & 0 & 0 & -\omega_s(L_{sW}+L_I)J_2 & 0 & -Mi_F & -\mu_I\\ 0 & 0 & 0 & 0 & 0 & 0 & \mu_W\\ 0 & 0 & 0 & M^Ti_F & 0 & 0 & 0\\ \mu_I^T & -\mu_D^T & 0 & \mu_I^T & -\mu_W & 0 & 0\end{bmatrix} \tag{39}$$

$$\mathcal{R}=\begin{bmatrix}(R_{sD}+R_I)I_2 & 0 & 0 & R_II_2 & 0 & 0 & 0\\ 0 & R_rI_2 & 0 & 0 & 0 & 0 & 0\\ 0 & 0 & B_D & 0 & 0 & 0 & 0\\ R_II_2 & 0 & 0 & (R_{sW}+R_I)I_2 & 0 & 0 & 0\\ 0 & 0 & 0 & 0 & R_F & 0 & 0\\ 0 & 0 & 0 & 0 & 0 & B_W & 0\\ 0 & 0 & 0 & 0 & 0 & 0 & R_B\end{bmatrix} \tag{40}$$

As expected when modeling power converters in the port-controlled Hamiltonian framework, the switching control actions (μ_D, μ_W and μ_I) appear in the interconnection matrix (39), see [22] for further details.

4. Bond graph model

Many electrical machines are described using the bond graph approach. From the DC machine [13] or AC generator [23], to three-phase induction machines [21,24]. HEV are also modeled using this graphic tool. In [25] a complete bond graph model for a long urban transit bus is obtained and simulated. A bond graph model of a parallel HEV system is presented in [26]. In that case, the electrical machine and internal combustion engine were modeled as an ideal torque sources (Se-element), while the main contribution was focused in the transmission, aerodynamics and wheel models.

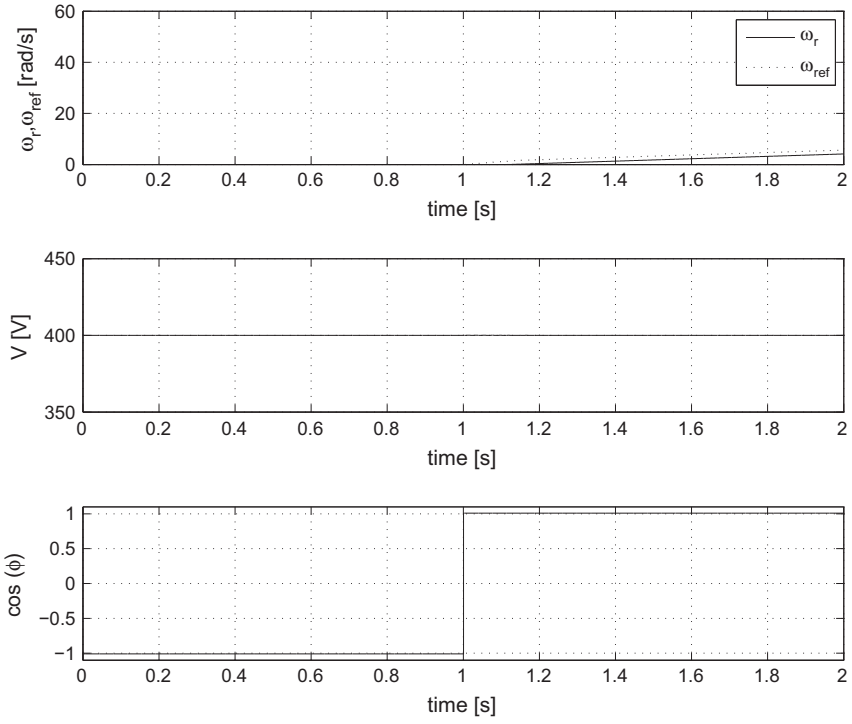

Fig. 12. Simulation results: DFIM mechanical speed and its reference, Stator voltage amplitude (V) and Stator Power Factor.

Exploiting the network based modeling of the bond graph approach, the whole model of the proposed series HEV DiSAC configuration is obtained by linking the different subsystems.

The bond graph models of the DFIM, the WRSM and the power converter are depicted in Figs. 5–7, respectively. For these models the following I-elements L_{lsD}, L_{lr}, L_{lsW}, L_{lF} are defined as

$$L_{lsD} = L_{sD} - L_{sr}$$

$$L_{lr} = L_r - L_{sr}$$

$$L_{lsW} = L_{sW} - L_m$$

$$L_{lF} = L_F - L_m.$$

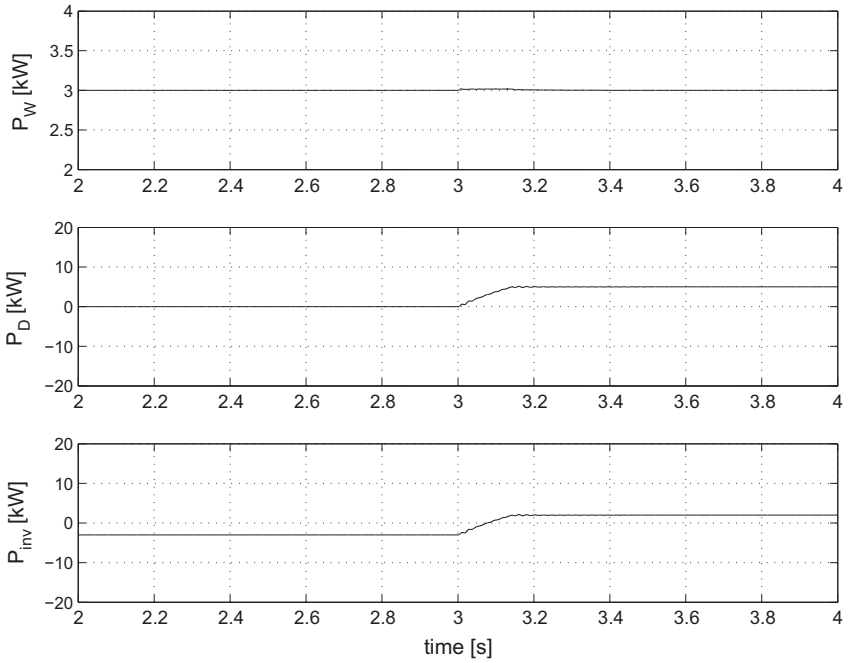

Fig. 13. Simulation results: WRSM (P_W), DFIM (P_D) and stator converter (P_{inv}) electrical powers.

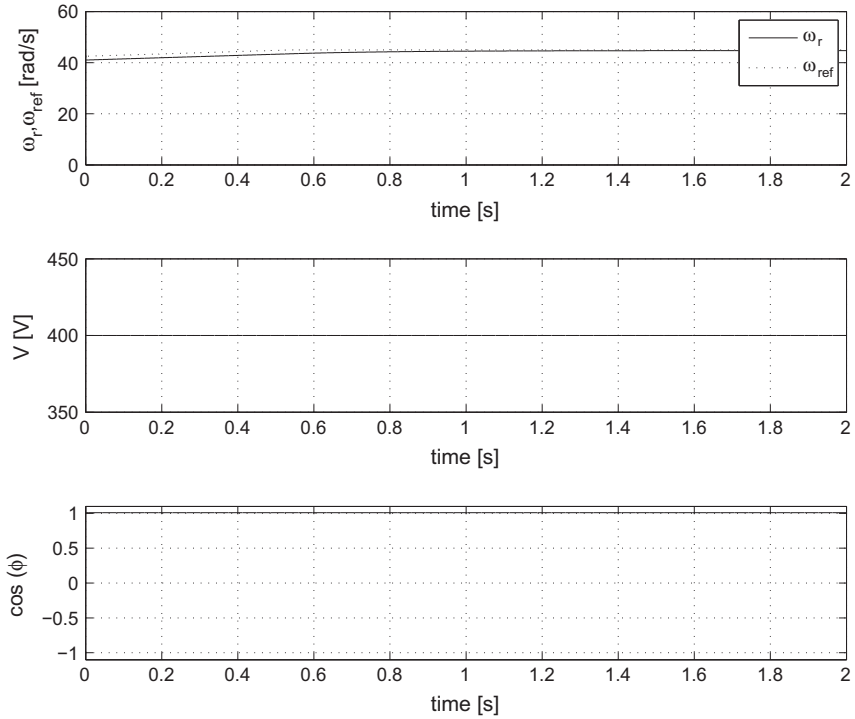

Fig. 14. Simulation results: DFIM mechanical speed and its reference, Stator voltage amplitude (V) and Stator Power Factor.

The battery is modeled as a nonlinear capacitor with a resistance emulating the self-discharge property, see in Fig. 8 the corresponding bond graph. A complex models of batteries can be found in the literature, see examples in [27] and [28] for lead–acid and lithium–ion batteries, respectively. Both can be used, directly replacing the bong graph of Fig. 8.

Linking the WRSM, the DFIM and the DC–AC inverter through the stator side of both machines, and connecting the battery by means of the DC–DC and DC–AC power converters, the whole model is obtained, see Fig. 9. In this case, power converters are modeled as a modulated transformer, MTF, which represents de averaged duty-cycle of the switches, [29]. Also, multi-bonds are used for the dq-coordinates in order to simplify the bond graph.

As a consequence of linking the power converter with the WRSM and the DFIM the I-elements of the stator inverter, in Fig. 7, are now with a non-preferred causality. This corresponds to the current constraint given by (33).

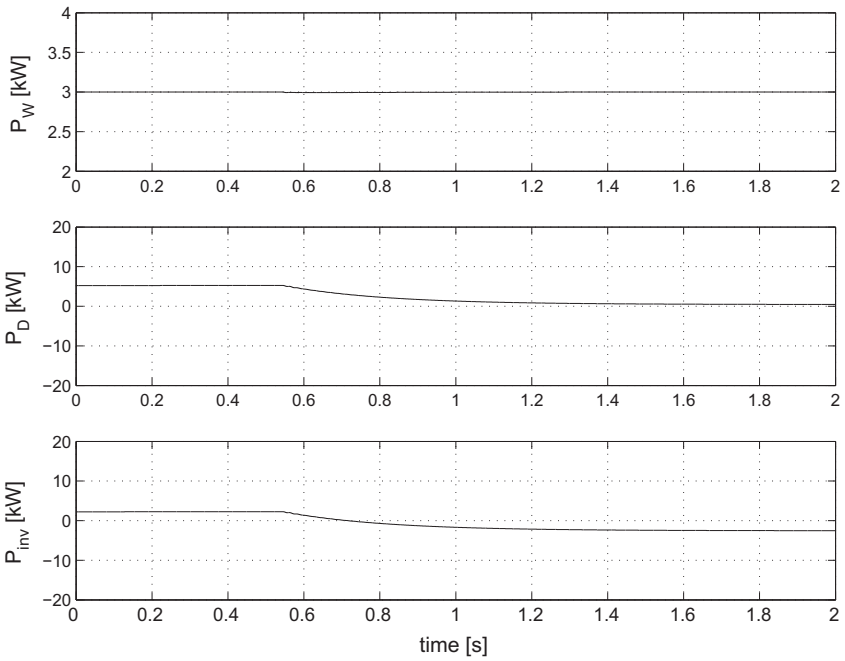

Fig. 15. Simulation results: WRSM (P_W), DFIM (P_D) and stator converter (P_{inv}) electrical powers.

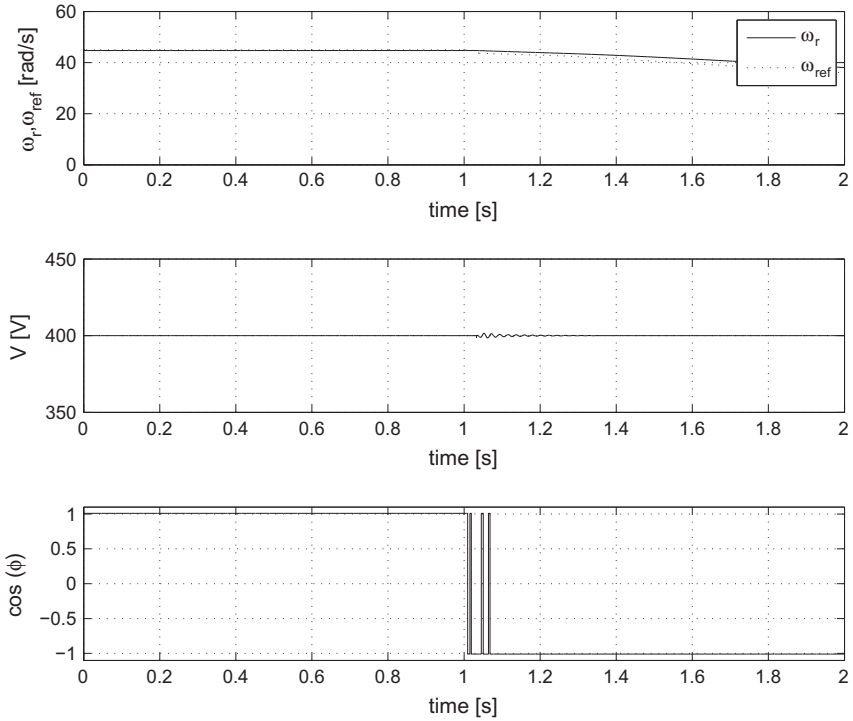

Fig. 16. Simulation results: DFIM mechanical speed and its reference, Stator voltage amplitude (V) and Stator Power Factor.

5. Vehicle model

The DiSAC power train system is tested as a propulsion system for an HEV. To this end, the bond graph model of the DiSAC system can be connected to the vehicle dynamics through the mechanical port of the DFIM. As mentioned above, the bond graph technique is specially attractive for linking easily different subsystems.

The vehicle dynamics is modeled as a mass, M, subjected to different forces, see Fig. 10. As a first approach there are considered the propulsion force, F_P, the effects associated with the rolling resistance,

$$F_{roll} = CMgv, \tag{41}$$

and with the slope of the road,

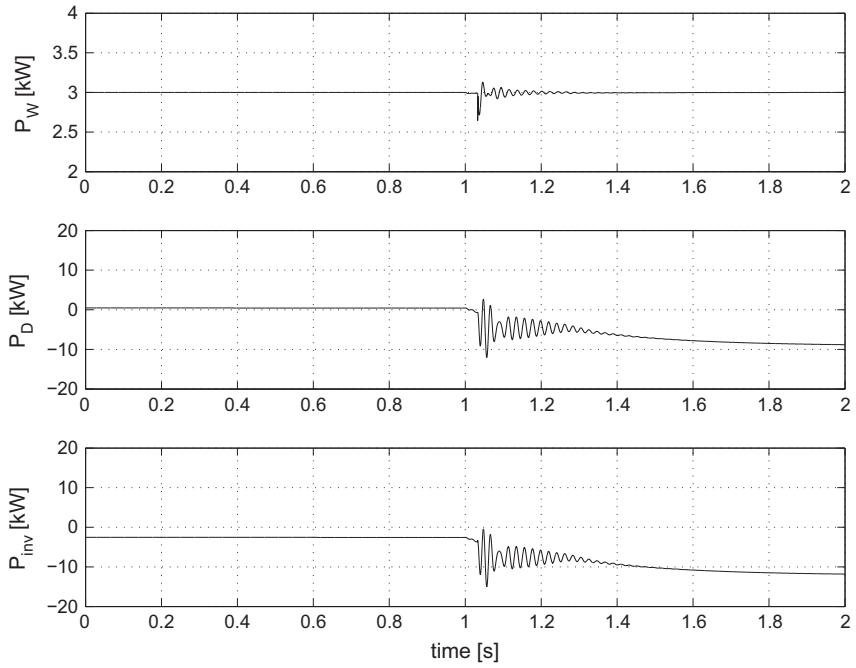

Fig. 17. Simulation results: WRSM (P_W), DFIM (P_D) and stator converter (P_{inv}) electrical powers.

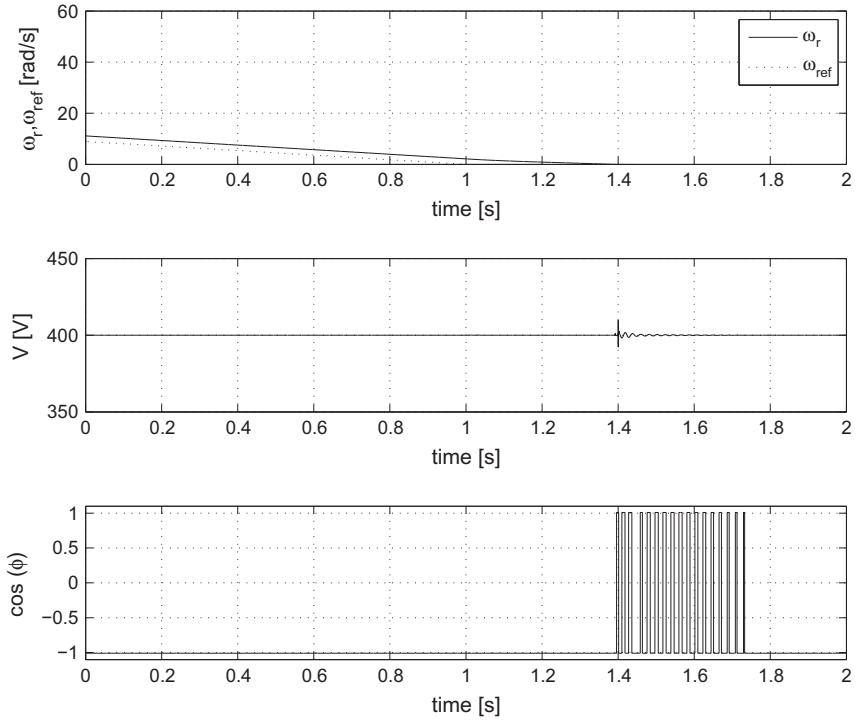

Fig. 18. Simulation results: DFIM mechanical speed and its reference, Stator voltage amplitude (V) and Stator Power Factor.

$$F_{slo} = Mg \sin \Theta, \tag{42}$$

where C is the coefficient of the rolling resistance, g is the gravitational acceleration, v is the vehicle speed and Θ is the road angle measured with respect to the horizontal. This model can be improved considering the aerodynamic drag and the wheel bearing losses [30].

Furthermore, there are considered the transformation from the angular dynamics to the translational one (which depends on the radius of the wheels, r) and the vehicle transmission, r_{trans}, which scales the torque and speed through the differential and the transmission ratio and is considered lossless.

The bond graph of the vehicle dynamics is depicted in Fig. 11. It consists in a I-element (with the mass of the vehicle), a dissipative R-element, which models the rolling resistance, and an external Se-source with the gravitational effect in case of certain slope of the road. The two TF-elements model the transformation from the angular dynamics (the wheels) and the transmission and differential ratio.

The complete system for simulation purposes, which includes the DiSAC power train with the vehicle dynamics is obtained by

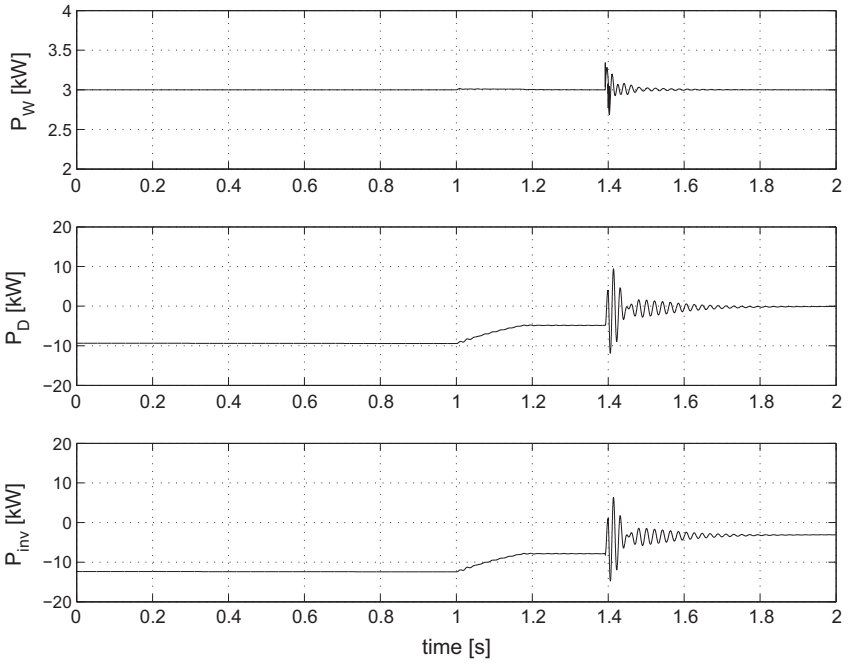

Fig. 19. Simulation results: WRSM (P_W), DFIM (P_D) and stator converter (P_{inv}) electrical powers.

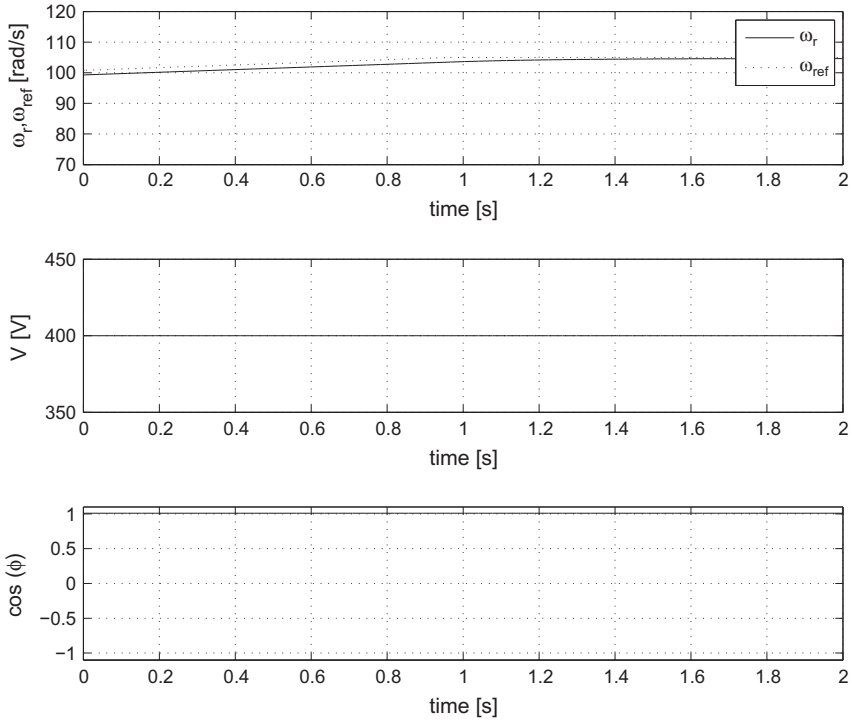

Fig. 20. Simulation results: DFIM mechanical speed and its reference, Stator voltage amplitude (V) and Stator Power Factor.

linking the bond graph in Figs. 9 and 11 trough the bonds corresponding to the torque of the DFIM and the vehicle, τ_D and τ_P, respectively.

6. Simulation results

In this Section numerical simulations are presented in order to test the proposed power train. The WRSM was controlled via a PI controller. The DFIM uses a current PI controller, designed accordingly to [31]. A PI control outer loop emulates the driver action and provides the torque reference to track the desired speed. The stator inverter is also controlled via a PI loop. Simulations were performed using the 20sim software which contains a bond graph editor.

The machines rated power are $P_W = 8.1$ kVA and $P_D = 15$ kVA. The DFIM and WRSM parameters are $R_{sD} = 0.2147\ \Omega$, $R_r = 0.2205\ \Omega$, $L_s = 65.181$ mH, $L_r = 65.181$ mH, $L_{sr} = 64.19$ mH,

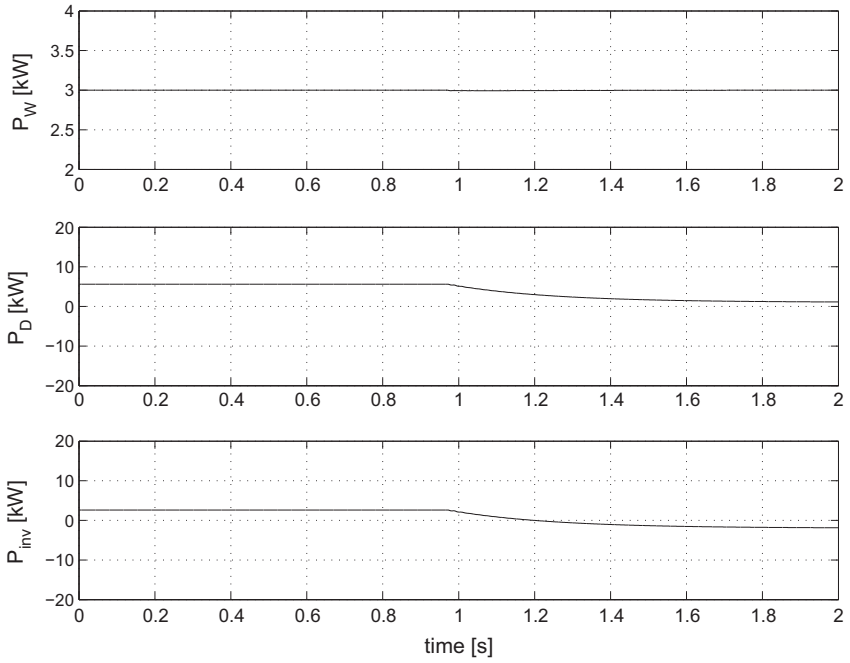

Fig. 21. Simulation results: WRSM (P_W), DFIM (P_D) and stator converter (P_{inv}) electrical powers.

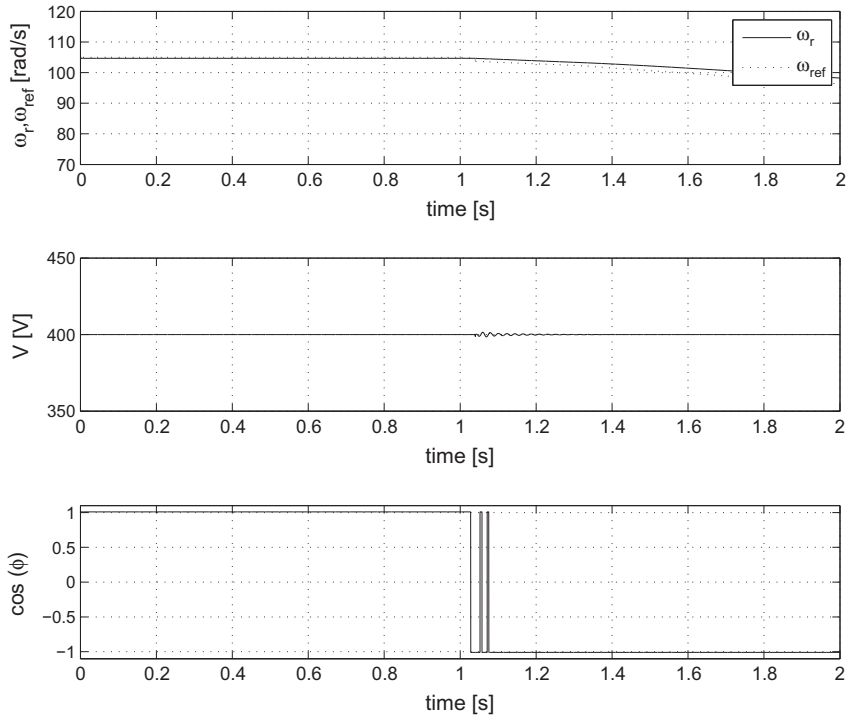

Fig. 22. Simulation results: DFIM mechanical speed and its reference, Stator voltage amplitude (V) and Stator Power Factor.

$J_D = 0.102$ Kg m^2, $B_D = 0.009541$ Nm rad^{-1} s^{-1}, and $L_{sW} = 113.127$ - mH, $R_{sW} = 1.62\ \Omega$, $L_m = 108.6$ mH, $L_F = 109.92$ mH, $R_F = 1.208$ H and the WRSM mechanical speed is fixed at $\omega = 314$ rad s^{-1}. The stator inverter inductance is set to $L_I = 4$ mH with a parasitic resistor of $R_I = 0.1\ \Omega$. The transmission and differential ratio are set to 1 and 4, respectively. The battery parameters are: $b_1 = 0.1$, $b_2 = 1 \times 10^{-6}$, $b_3 = 0.9$, and $b4 = 700$. The control parameters are $K_p = 20$, $K_i = 3$ (for the WRSM) and $K_p = 1$, $K_i = 0.01$ (DFIM). The speed control parameters are $K_p = 10$ and $K_i = 0.05$. Finally, the stator power converter control gain parameters are $K_p = 0.1$, $K_i = 1$.

The control objectives are to regulate the stator voltage ($V = 400$ V), the WRSM output power ($P_s = 3$ kW), the DFIM mechanical speed (ω_r), and to keep an unitary DFIM stator power factor. Several reference speed changes, namely, increase and

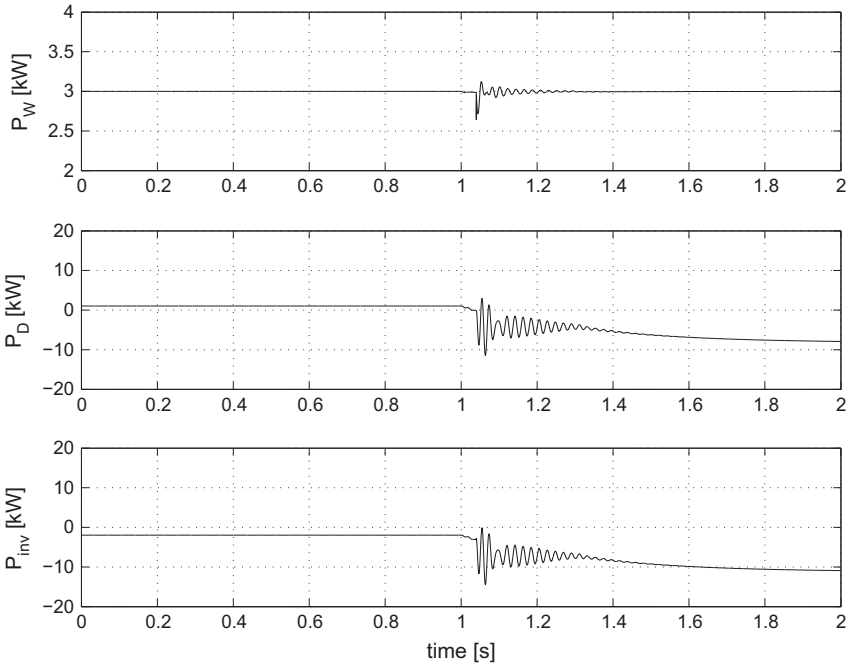

Fig. 23. Simulation results: WRSM (P_W), DFIM (P_D) and stator converter (P_{inv}) electrical powers.

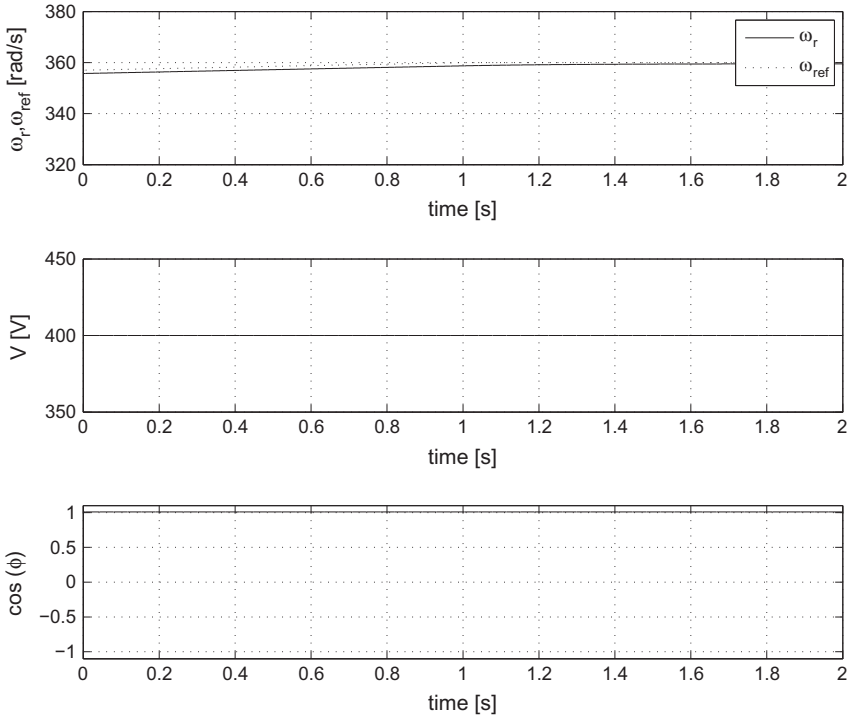

Fig. 24. Simulation results: DFIM mechanical speed and its reference, Stator voltage amplitude (V) and Stator Power Factor.

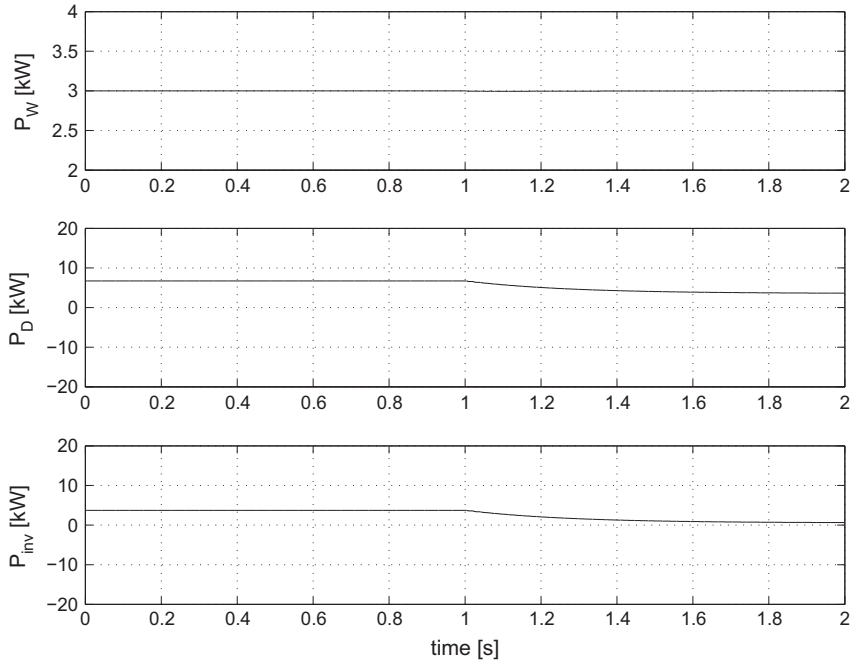

Fig. 25. Simulation results: WRSM (P_W), DFIM (P_D) and stator converter (P_{inv}) electrical powers.

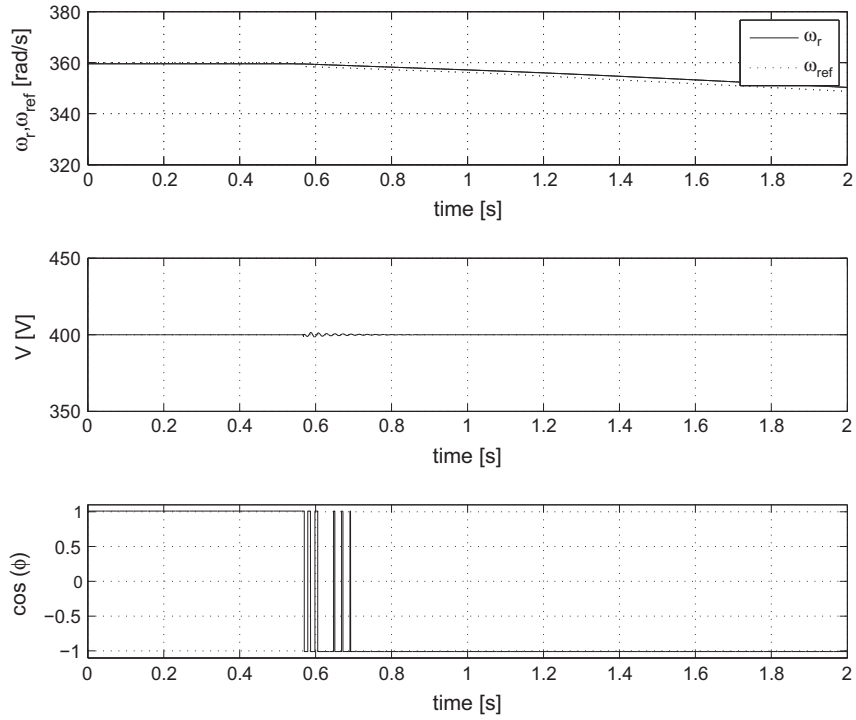

Fig. 26. Simulation results: DFIM mechanical speed and its reference, Stator voltage amplitude (V) and Stator Power Factor.

decrease reference speed at low, medium and high speed, have been set in order to show the different power flow conditions.

Figs. 12, 14, 16, 18, 20, 22, 24 and 26 show in the upper the DFIM mechanical speed and its reference (both were referenced to machine speed, for this reason the unities are rad s^{-1}); in the middle the stator voltage amplitude and in the bottom the DFIM stator power factor (PF).

Figs. 13, 15, 17, 19, 21, 23, 25 and 27 show the electrical power flow trough the DFIM stator side, P_{sD}, SM stator windings, P_{sW}, and the inverter, P_I.[4] As explained before, the rotor active power changes is bidirectional and allows to store energy into the batteries. In this case the battery state of charge (SOC) is not taken into account. For further development when the battery reaches to the maximum allowed SOC, either, an electrical or mechanical brake must exist.

[4] In the dq coordinates, the instantaneous active and reactive power can be computed as $P_r = v_r^T i_r$ and $Q_s = v_s^T J_2 i_s$.

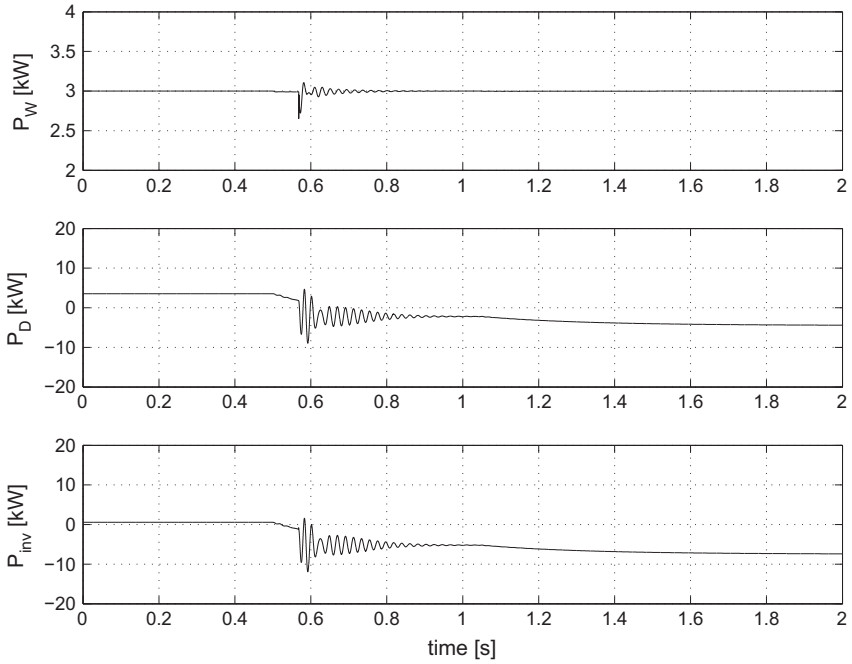

Fig. 27. Simulation results: WRSM (P_W), DFIM (P_D) and stator converter (P_{inv}) electrical powers.

From Figs. 12–19 represent the system behavior at low speed, while Figures from Figs. 20–23 and from Figs. 24–27 represent them for medium and high speed, respectively. The speed reference changes were extracted from the NEDC (New European Driving Cycle) profile.

As a result, note how the control objectives are reached and the power flow through the proposed DiSAC system can be controlled. In this work a power limit was not imposed to the stator converter, neither absorbing nor providing power. In future works this power limitations will be studied, together with the power ratio of each converter The control design is also a future study case.

Note that the DFIM stator PF remains close to ±1 when the stator power of the DFIM is positive or negative, respectively (i.e., when the machine is providing power to the wheels or it is in regenerative braking). When the vehicle is stopped PF = 0 due to the magnetization losses.

In Fig. 13 the DFIM accelerates from zero to low speed. The inverter starts absorbing approximately the amount of power generated by WRSM, while the power consumed by the DFIM is close to zero. Subsequently, after the transient, the DFIM absorbs the power provided by both the inverter and the WRSM. Fig. 19 corresponds to the case in which the machine decelerates from low speed to zero.

The result of the DFIM accelerating at low speed is presented in Fig. 15. The inverter starts providing electrical power from the batteries, while the DFIM absorbs such power together with the one generated by the WRSM. After the transient, at constant speed, the power consumed by the DFIM is lower than the power generated by the WRSM. Note that the extra amount of power is absorbed by batteries trough the inverter. Fig. 17 corresponds to the case in which the machine decelerates at low speed.

Figs. 21 and 23 present the acceleration and deceleration of DFIM at medium speed, respectively. During the acceleration, the batteries provides the extra power consumption of the DFIM, whereas at constant speed the batteries stores the extra power generated by the WRSM, the deceleration process is complementary.

Finally, Figs. 25 and 27 present the acceleration and deceleration of DFIM at high speed, respectively. At this speed, the power consumption of the DFIM is very high either at constant speed or accelerating, then, both the WRSM and the batteries provide all the energy. On the other hand, during the decelerating part, the energy is stored into the batteries.

In optimal conditions, the SOC can be regulated by adjusting the WRSM generated power, but it is out of the scope of this paper and it will be studied in future works.

7. Conclusions

An alternative architecture for a series HEV propulsion system has been proposed. It is composed by two wounded rotor machines (WRSM and DFIM) directly connected through the stator, with a DC/AC converter. The advantage of this topology is that the required power converters are smaller than other series configurations [4].

The complex system under study has been divided into several subsystems; the WRSM, the DFIM the power inverter, the batteries and the required DC–DC and DC–AC power converters. Two energy-based models have been presented, following the Hamiltonian formalism and the bond graph approach, and the whole system is obtained by linking the submodels. As additional feature, the submodel integration capability, inherent to bond graph technique, allows to easily expand the proposed model, by interconnection with other mechanical (transmission, wheels, aerodynamics, etc.) and electrical parts (discrete power converters, complex battery models, etc.), in future works. Moreover, from a control viewpoint, the presented PCH model will be of great help to design passivity-based controllers.

The proposed models of the novel series HEV topology has been comprehensively assessed through simulations, showing satisfactory results. The proposed DiSAC system can be fully controlled.

Future works include the control design for the different system stages and the energy management policy of the whole system.

Acknowledgment

R.S. Muñoz-Aguilar, A. Dòria-Cerezo and P.F. Puleston were partially supported by the Spanish government research projects ENE2011-29041-C02-01, DPI2010-15110 and Marie Curie FP7-PIIF-911767 (EU), CONICET and UNLP (Argentina), respectively.

References

[1] Emadi A, Rajashekara K, Williamson SS, Lukic SM. Topological overview of hybrid electric and fuel cell vehicular power system architectures and configurations. IEEE Trans Vehic Technol 2005;54(3):763–70.
[2] Bayindir K, Gozukucuk MA, Teke A. A comprehensive overview of hybrid electric vehicle: powertrain configurations, powertrain control techniques and electronic control units. Energy Convers Manag 2011;52(2):618–28.
[3] Lidozzi A, Solero L, Di Napoli A. Ultracapacitors equipped hybrid electric microcar. IET Electr Power Appl 2010;4(8):618–28.
[4] Miller JM. Propulsion systems for hybrid vehicles. IEE, Power Energy Ser 2004.
[5] Caratozzolo P, Fossas E, Pedra J, Riera J. Dynamic modeling of an isolated motion system with dfig. In: Proceedings of the VII IEEE international power electronics congress; 2000. p. 287–92.
[6] Ortmeyer T. Variable voltage variable frequency options for series hybrid vehicles. In: Proceedings of IEEE conference on vehicle power and propulsion; 2005. p. 262–7.
[7] Muñoz-Aguilar RS, Dòria-Cerezo A, Puleston PF. Energy-based modelling and simulation of a series hybrid electric vehicle propulsion system. In: Proceedings of the European control conference; 2009.
[8] Ducusin M, Gargies S, Mi Chunting. Modeling of a series hybrid electric high-mobility multipurpose wheeled vehicle. IEEE Trans Vehic Technol 2007;56(2):557–65.
[9] Antoniou AI, Komyathy J, Bench J, Emadi A. Modeling and simulation of various hybrid-electric configurations of the high-mobility multipurpose wheeled vehicle (hmmwv). IEEE Trans Vehic Technol 2007;56(2):459–65.
[10] Willems JC. The behavioral approach to open and interconnected systems. IEEE Control Syst Magaz 2007;27(6):46–99.
[11] van der Schaft A. L_2 gain and passivity techniques in nonlinear control. Springer; 2000.
[12] Duindam V, Macchelli A, Stramigioli S, Bruyninckx H, editors. Modeling and control of complex physical systems: the port-hamiltonian approach. Springer; 2009.
[13] Karnopp D, Margolis D, Rosenberg R. System dynamics: modeling and simulation of mechatronic systems. John Wiley and Sons, Inc; 2006.
[14] Chan CC, Bouscayrol A, Chen K. Electric, hybrid, and fuel–cell vehicles: architectures and modeling. IEEE Trans Vehic Technol 2010;59(2):589–98.
[15] Ehsani M, Gao Y, Gay SE, Emadi A. Modern electric, hybrid electric, and fuel cell vehicles: fundamentals, theory, and design. Boca Raton, FL: CRC; 2004.
[16] Ceraolo M, di Donato A, Franceschi G. A general approach to energy optimization of hybrid electric vehicles. IEEE Trans Vehic Technol 2008;57(3):1433–41.
[17] Muñoz Aguilar RS. Modeling and simulation of a series hybrid electric vehicle propulsion system. Master's thesis, Universitat Politecnica de Catalunya; 2010.
[18] Krause P, Wasynczuk O, Sudhoff S. Analysis of electric machinery and drive systems. John-Wiley and Sons; 2002.
[19] Batlle C, Dòria-Cerezo A, Ortega R. Power flow control of a doubly–fed induction machine coupled to a flywheel. Euro J Control 2005;11(3):209–21.
[20] Guo Y, Xi Z, Cheng D. Speed regulation of permanent magnet synchronous motor via feedback dissipative hamiltonian realization. IET Control Theory Appl 2007;1(1):281–90.
[21] Batlle C, Dòria-Cerezo A. Energy-based modeling and simulation of the interconnection of a back-to-back converter and a doubly-fed induction machine. In: American control conference; 2006. p. 1851–6.
[22] Escobar G, van der Schaft AJ, Ortega R. A hamiltonian viewpoint in the modeling of switching power converters. Automatica 1999;35(3):445–52.
[23] Batlle C, Dòria-Cerezo A. Bond graph models of electromechanical systems. The ac generator case. In: IEEE international symposium on industrial electronics; 2008.
[24] Kim J, Bryant M. Bond graph model of a squirrel cage induction motor with direct physical correspondence. J Dynam Syst Measur Control 2000;22:461–9.
[25] Hubbard G, Youcef-Toumi K. Modeling and simulation of a hybrid-electric vehicle drivetrain. In: Proceedings of the 1997 American control conference, vol. 1; 1997. p. 636–40.
[26] Filippa M, Mi C, Shen J, Stevenson C. Modeling of a hybrid electric vehicle powertrain test cell using bond graphs. IEEE Trans Vehic Technol 2005;54(3):837–45.
[27] Esperilla JJ, Felez J, Romero G, Carretero A. A model for simulating a lead–acid battery using bond graphs. Simul Modell Practice Theory 2007;15:82–97.
[28] Menard L, Fontes G, Astier S. Dynamic energy model of a lithium–ion battery. Math Comput Simul 2010;81:327–39.
[29] Delgado M, Sira-Ramirez H. A bond graph approach to the modeling and simulation of switch regulated dc-to-dc power supplies. Simul Practice Theory 1998;6(7):631–46.
[30] Dhameja S. Electric vehicle battery systems. Butterworth-Heinemann; 2002.
[31] Batlle C, Dòria-Cerezo A, Ortega R. A robustly stable pi controller for the doubly-fed induction machine. In: Proceedings of IEEE industrial electronics conference; 2006.